journal

J. Am. Ceram. Soc., 93 [8] 2359–2368 (2010)
DOI: 10.1111/j.1551-2916.2010.03717.x


# Internal Residual Stress Measurements in a Bioactive Glass–Ceramic Using Vickers Indentation

Oscar Peitl,[‡] Francisco C. Serbena,[†,§] Valmor R. Mastelaro,[¶] and Edgar D. Zanotto[‡]

[‡]Vitreous Materials Laboratory (LaMaV), Department of Materials Engineering (DEMa), Federal University of São Carlos (UFSCar), CEP 13565-905, São Carlos, SP, Brazil

[§]Department of Physics, State University of Ponta Grossa (UEPG), CEP 84030-900, Ponta Grossa, PR, Brazil

[¶]Physics Institute of São Carlos, State University of São Paulo (USP-São Carlos), CEP 13560-970, São Carlos, SP, Brazil

**The residual stress distribution that arises in the glass matrix during cooling of a partially crystallized $17.2Na_2O$–$32.1CaO$–$48.1SiO_2$–$2.5P_2O_5$ (mol%) bioactive glass–ceramic was measured using the Vickers indentation method proposed by Zeng and Rowcliffe (ZR). The magnitude of the determined residual stress at the crystal/glass boundary was 1/4–1/3 of the values measured using X-ray diffraction (within the crystals) and calculated using Selsing's model. A correction for the crack geometry factor, assuming a semi-elliptical shape, is proposed and then good agreement between experimental and theoretical values is found. Thus, if the actual crack geometry is taken into account, the indentation technique of ZR can be successfully used. In addition, a numerical model for the calculation of residual stresses that takes into account the hemispherical shape of the crystalline precipitates at a free surface was developed. The result is that near the sample surface, the radial component of the residual stress is increased by 70% in comparison with the residual stress calculated by Selsing's model.**

## I. Introduction

Biomaterials development has been focused on materials that match the bio-mechanical properties of bone and have sufficient bioactivity to bond to living bone and soft tissue.[1–4] An approach to improve the mechanical properties of bioactive glasses is by controlled crystallization and the development of glass–ceramics, such as the A/W glass–ceramic (Cerabone), pioneered by Yamamuro and Kokubo.[3] The high strength and toughness of Cerabone makes it a successful load-bearing replacement for cortical bone. However, its modulus of elasticity is one order of magnitude higher than that of cortical bone giving rise to the possibility of long-term stress shielding when the material is used as a bone replacement.[4] Also, its low level of bioactivity is insufficient for bonding to soft connective tissues,[4] as needed for some clinical applications.

In a previous work with glasses within the composition range $1Na_2O$–$2CaO$–$3SiO_2$ and $1.5Na_2O$–$1.5CaO$–$3SiO_2$, some of us have shown that crystallization slows down, but does *not* inhibit the development of a crystalline hydroxyl–carbonate apatite at the material/bone interface. The resulting glass–ceramics show a similar level of bioactivity as the "golden standard" 45S5 Bioglass®[1,2] developed by Professor Larry Hench. The main aim now is to optimize the mechanical properties of these glass–ceramics, which are strongly dependent on the material's microstructure and internal residual stresses.

Internal residual stresses arise in glass–ceramics on cooling down from the crystallization temperature due to thermal expansion and elastic mismatch between the crystalline and the glassy phase. Therefore, the fracture strength of these materials strongly depends on their microstructure and type (tension or compression) and the magnitude of these residual stresses.

Different experimental techniques, such as X-ray diffraction,[5] Raman spectroscopy,[6] and nuclear magnetic resonance[7] have been used to measure residual stresses in the *crystalline phase* of glass–ceramics.

A simple technique to measure the residual stress field in the *glass phase* in principle was proposed by Zeng and Rowcliffe.[8–10] The basis of this technique is as follows: when a Vickers indentation is made with a moderate load on the surface of a stress-free glass sample, a permanent impression is formed and four symmetrical radial cracks of equal length arise from the corners of the generated impression. In addition, a residual stress field is created around the indentation. Zeng and Rowcliffe[8–10] observed that this residual stress field is an unequal bi-axial field, with a tensile stress in the tangential direction and compressive stress in the radial direction with respect to the indentation. If a second indentation is made near the first, the crack pattern and crack length of the second indentation will be affected by the residual stress field of the first. By measuring the lengths of the secondary cracks, and comparing them with the crack length developed at the same load in a stress-free surface, the residual field around the first indentation can be calculated using a simple analysis.

Previously, some of us reported an experimental test of Selsing's model,[11] which is often used to describe the residual stresses around a second phase, using a partially crystallized soda–lime–silica glass with the same chemical composition of the glass used in this work.[5] In that study, an average value of the residual stress field around crystals embedded in the glass matrix for a particular set of *hkl* plane was measured ($\sim$150 MPa). Good agreement between experimental results and calculation was found.

In the present work, we tested the indentation technique of Zeng and Rowcliffe[8–10] to estimate the residual stress field in the glass matrix (around crystals embedded in the same glass used in Peitl *et al.*[1]). In this case, the crystals play the role of the primary indentation that generates residual stress. The results are compared with those obtained using X-ray diffraction experiments and theoretical modeling for the crystalline particles. In the end, a new crack geometry factor is proposed to be used in the ZR model considering the semi-elliptical shape of the generated cracks. In addition, a numerical model for the calculation of residual stress, which takes into account the hemispherical shape of a crystalline precipitate at a free surface, is developed.

V. Sglavo—contributing editor

Manuscript No. 26756. Received August 27, 2009; approved February 4, 2010.
[†]Author to whom correspondence should be addressed. e-mail: fserbena@uepg.br

## II. Theory

### (1) Residual Stress Calculation Using the Indentation Technique

In order to calculate the residual stress around an indentation, Zeng and Rowcliffe[8] considered first an indentation made in a stress-free material. In this case, the radial crack length of the indentation is related to the material's toughness $K_c$ by the following expression:

$$K_c = \chi_r \frac{P}{c_0^{3/2}} \tag{1}$$

where $K_c$ is the stress intensity factor at the indentation crack tip, $P$ is the indentation load, $c_0$ is the crack length, and $\chi_r$ is a dimensionless constant, which is related to the ratio of the elastic modulus to hardness. If a second indentation is made near the first one, the crack that originated from the second indentation will be $c_1$ (where $c_0 < c_1$) because of the effect of the residual tensile stress from the first indentation, or $c_2$ (where $c_0 > c_2$) because of the effect of the compressive stress from the first indentation. If the stress intensity factor at the new crack tip is still $K_c$, then Eq. (1) becomes[8,9]:

$$K_c = \chi_r \frac{P}{c_1^{3/2}} + \Phi\sigma_t c_1^{1/2} \text{ (for tensile stress)} \tag{2a}$$

$$K_c = \chi_r \frac{P}{c_2^{3/2}} - \Phi\sigma_c c_2^{1/2} \text{ (for compressive stress)} \tag{2b}$$

where $\Phi$ is the crack geometry factor, a constant related to the crack geometry and loading condition and was assumed to be equal to $\pi^{1/2}$ because the problem treated by Zeng and Rowcliffe was simplified to a plane stress problem. Their model also assumes that, if the secondary crack is small, both tensile and compressive stresses are constant over the secondary crack. By substituting $\chi_r$ from Eq. (1) in Eq. (2), the following expressions can be obtained for the tensile and compressive residual stress[8,9]:

$$\sigma_r = K_c \frac{1 - (c_0/c_1)^{3/2}}{\Phi c_1^{1/2}} \text{ (for tensile stress)} \tag{3a}$$

$$\sigma_r = -K_c \frac{1 - (c_0/c_2)^{3/2}}{\Phi c_2^{1/2}} \text{ (for compressive stress)} \tag{3b}$$

Zeng and Rowcliffe used Eqs. (3*a*) and (3*b*) to calculate the residual stress at any point around the first indentation from measurements of the crack length changes at the second indentation.

### (2) Residual Stress Calculation by Selsing's Model

The theory concerning stresses around an isolated particle in an isotropic medium is well established.[11] Because the thermal expansion coefficients of the two phases are generally different, stresses are set up within and around the particles as the body cools down below the glass transition temperature. An isotropic spherical particle will be subjected to a pressure $P$, and the matrix will be subjected to radial and tangential stresses of:

$$\sigma_r = P\frac{a^3}{r^3} \text{ (radial stress)} \tag{4a}$$

$$\sigma_t = -\frac{P}{2}\frac{a^3}{r^3} \text{ (tangential stress)} \tag{4b}$$

where $a$ is the crystal radius and $r$ is the distance from a point in the matrix to the center of the particle. For an isotropic system containing several particles in a matrix, Eq. (4) should still hold if the stress fields around each particle do not overlap. This situation is expected to be valid if the volume percentage of the second phase does not exceed approximately 15%.[12] Thus, these stresses are maximum at the crystal/glass interface ($r = a$) and drop to only 3.7% of the maximum for $r = 4a$. The hydrostatic thermal stress, $P$, can be obtained by the following equation[11,12]:

$$P = \Delta\alpha\Delta T/K_e \tag{5}$$

where $K_e = [(1 + \upsilon_m)/2E_m + (1 - 2\upsilon_p)/E_p]$, $E$ and $\nu$ being, respectively, the elastic modulus and the Poisson ratio, and the subscripts, m and p, refer to the matrix and particle, respectively. $\Delta\alpha = \alpha_p - \alpha_m$ is the thermal expansion mismatch and $\Delta T$ is the difference between the temperature at which the glass ceases to flow on cooling ($\approx T_g$) and the ambient temperature.

According to previous work,[5] the crystals present in this particular glass–ceramic have an average thermal expansion coefficient higher than that of the glass matrix, meaning that the crystals are under hydrostatic tensile stresses and the expected stress distribution in the matrix is shown in Fig. 1. Hence, near the crystals, where the indentations are applied, the matrix will be subjected to tensile stresses in the radial direction and compressive stresses in the tangential direction, meaning that the indentation cracks that are parallel to the glass/crystal interface will be extended due to the influence of the tensile residual stress and vice versa. Figure 1 shows a schematic diagram of the indentation system and how the crack pattern generated at a small secondary indent is affected by the residual stress around a large precipitate.

## III. Experimental Procedure

### (1) Material Preparation

A $17.2Na_2O$–$32.1CaO$–$48.1SiO_2$–$2.5P_2O_5$ (mol%) glass was prepared by melting a homogeneous mixture of reagent-grade $Na_2CO_3$, $CaCO_3$, $SiO_2$, and $P_2O_5$ at 1400°C for 3 h in a Pt crucible. This chemical composition is the same as the glass used in Mastelaro and Zanotto.[5] The melt was then cast between two cold steel plates, with an estimated cooling rate of 400°C/min. To obtain partially crystallized glasses, a specimen was submitted to an isothermal treatment at 840°C for a period of 28 min, followed by annealing at 540°C for 15 min. Microstructural analysis revealed that the average crystal radius and the crystallized volume fraction were $176 \pm 23$ μm and 4%, respectively.

### (2) Indentation Experiments

The crystallized surface of the specimen was removed by grinding with SiC. After polishing with 1 μm $CeO_2$ powder size, crystals embedded in the glass matrix were revealed by chemical etching in a solution of 0.08% HF–0.04% HCl. Before indentation, all samples were annealed at 555°C for 15 min, cooled

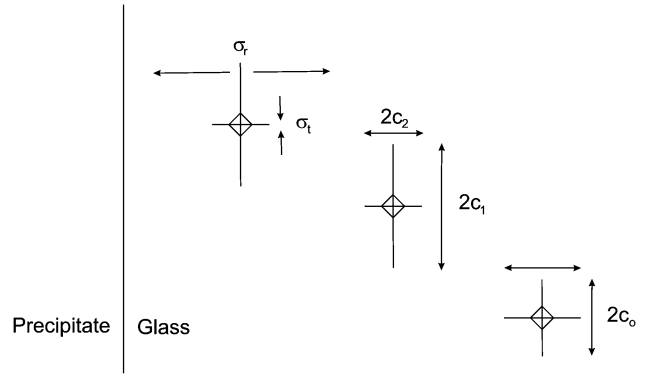


**Fig. 1.** Schematic diagram showing the indentation system and how the crack pattern at a small secondary indent is affected by the residual stress field around a large precipitate (adapted from Zeng and Rowcliffe[8]).

down to 515°C in 30 min, and slow cooled to room temperature at 10°C/min for the removal of any macroscopic residual stresses due to thermal gradients in the sample.

Indentations around the crystals were made using a Vickers diamond pyramid indenter using a digital microhardness tester model FM from Future-tech Corp. (Kawasaki, Japan) in a controlled environment of 20–22°C and 50%–70% air humidity. As proposed by Zeng and Rowcliffe,[8,9] the secondary indentation should be sufficiently small and made with low loads. In this work, a load of 0.5 N was used with a dwell time of 20 s. For comparison, Zeng and Rowcliffe[8,9] used loads between 2 and 7 N for the secondary indentations in soda–lime glass. The total number of indentations was 40.

The reference crack length $c_0$ was obtained at indentations made in the same sample in regions far from the crystals at a distance of approximately 800 μm. This distance is about 3.6 times greater than the radius of the larger crystal assuring the residual stresses were negligible.

The indentation crack lengths $c_1$ and $c_2$ were measured at indentations made around precipitates that were as close as possible to a hemispherical shape. Indentations were made at a distance of approximately 200 μm apart to avoid the influence of the mutual indentation stress field. Occasionally, when the indentation was very close to the precipitate/glass boundary, the radial cracks closer to the interface extended inwards the precipitate. Therefore, only the radial crack facing outward of the precipitate was measured and used to compute the tangential residual stress.

To evaluate the effect of water on crack indentation in this glass, two arrays of 10 indentations were performed in a remote region far from any precipitate. The indentations in one array were performed in air, while the indentations in the other array were performed immersed in distilled water. A load of 2 N was used with a dwell time of 20 s. The array performed in air was used to calculate the fracture toughness $K_c$ according to Niihara *et al.*[13]:

$$K_c = 0.035\left(\frac{l}{b}\right)^{-1/2}\left(\frac{H}{E\phi}\right)^{-2/5}\left(\frac{H\sqrt{b}}{\phi}\right) \tag{6}$$

where $H$ is the Vickers hardness, $b$ is the half-impression diagonal, $E$ is the elastic modulus, $l$ is $c$–$a$, and $\phi$ is a constant equal to 3.

A series of thirty 0.5 N indentations immersed in distilled water was performed around the precipitates to estimate the effect of the water environment when residual stresses were present. We also performed a series of at least eight 1 N indentations inside the precipitates of a partially crystallized sample and compared the measured crack lengths with the crack lengths of indentations on a fully crystallized sample to estimate the residual stresses.

In all situations, the crack lengths were measured immediately after indentation tests using an optical microscope in either transmission or reflection mode. The total time between the first indentation and the last crack length measured is estimated to be 2 h.

The indentation crack geometry was determined by performing a series of eight 0.5 N Vickers indentations in the surface of the bioglass–ceramic far from any precipitate in the same conditions as used in the stress determination tests. The radial crack geometry was established by hand polishing the glass surface in a $CeO_2$ and water solution and imaging the indentations by optical microscopy every 2 min.

A large Vickers indentation with a load of 5 N was performed near the smaller indentations to control the amount of surface removal during polishing. For Vickers indenter geometry, the diagonal/depth ratio is 7. Also, there is an elastic recovery of indentation depth after load removal, and for a soda–lime–silica glass, this is around 20%.[14] Therefore, by measuring the indentation diagonals at every step during polishing, the rate of surface removal was estimated.

### *(3) X-ray Diffraction Experiments*

To evaluate the residual stresses in the crystalline phase, X-ray diffraction experiments were performed at room temperature in the Bragg–Brentano mode with a Cu$K\alpha$ rotating anode tube. The recorded angular 2θ ranges were from 27° to 36° and from 46° to 52° in 0.02° steps to include the most intense peaks of the $Na_4Ca_4Si_6O_{18}$ crystal phase. During the measurements, the sample was rotated to avoid a possible effect of texture. To correct for errors in the peak positions, Si powder was deposited on the sample surface before testing, and was used as an internal reference. Rietveld refinement of the crystal structure was performed using the GSAS program[15] with the EXPGUI interface.[16] The phase was $Na_4Ca_4Si_6O_{18}$ with a hexagonal close-packed structure and *P312* symmetry space group.

During the refinement process using the GSAS program, the corrections for sample position errors were performed using the Si (111) and (220) peak positions. For this purpose, the Si powder lattice parameter was determined by Rietveld refinement from an X-ray diffraction pattern taken in the 2θ range from 20° to 90° at 0.02° steps. The Si lattice parameter and the diffractometer constants were then used as fixed parameters for the refinement of the $Na_4Ca_4Si_6O_{18}$ lattice parameter.

Strains and stresses were calculated from the change in the cell parameters of the crystalline phase $Na_4Ca_4Si_6O_{18}$ obtained by the refinement procedure by comparing bulk (stressed) and powder (unstressed) samples. But there is clear evidence that the lattice parameter of the crystalline phase in a similar glass varies with the crystallized volume fraction due to solid solution formation.[17,18] Therefore, in the indentation tests, we used a partially crystallized bulk sample ground to powder with a pestle and a mortar as a stress-free reference sample. Care was taken to remove the lateral crystallized surface by polishing before the X-ray experiments.

## IV. Results

### *(1) Indentation Experiments*

From the series of indentations with a 2 N load in air, a Vickers hardness $H$ of $5.9 \pm 0.4$ GPa and an average crack length of $47 \pm 2$ μm was measured. According to eq. (6) of Niihara *et al.*,[13] these values correspond to a fracture toughness of $0.65 \pm 0.02$ MPa · m$^{1/2}$. This value agrees with previous measurements in similar glasses.[19] A series of 10 indentations with a load of 0.5 N revealed a similar hardness, $6.1 \pm 0.4$ GPa, and a slightly lower value of indentation fracture toughness, $0.55 \pm 0.02$ MPa · m$^{1/2}$.

Surprisingly, water had no influence on the measured fracture toughness. The other series of 2 N indentations in water produced similar values, a hardness of $5.6 \pm 0.3$ GPa and a fracture toughness of $0.65 \pm 0.02$ MPa · m$^{1/2}$.

During these tests, indentations in the glass matrix around the precipitates were performed several times at different distances and at several angular positions and (within the precision of the indentation technique) we never observed any specific angular dependence of the measured residual stresses around a precipitate.

Figures 2(a) and (b) show typical indentations around a precipitate and far from its interface. The cracks parallel to the interface were longer than the perpendicular cracks, indicating that the radial residual stress component is tensile and the tangential component is compressive. A general overview of the indentation array around a precipitate is observed in Fig. 2(c). From measurements of crack lengths at several positions around the precipitates, the residual stress distributions were calculated according to Eqs. (3*a*) and (3*b*) as a function of the normalized distance $a/r$ and are shown in Figs. 3(a) and (b). The data show considerable scatter, but there is no significant difference between the stress profiles of indentations performed in air and water, confirming the results of the 2 N indentations. The stresses increase toward the precipitate and are significant only at a distance comparable with the diameter of the precipitate.

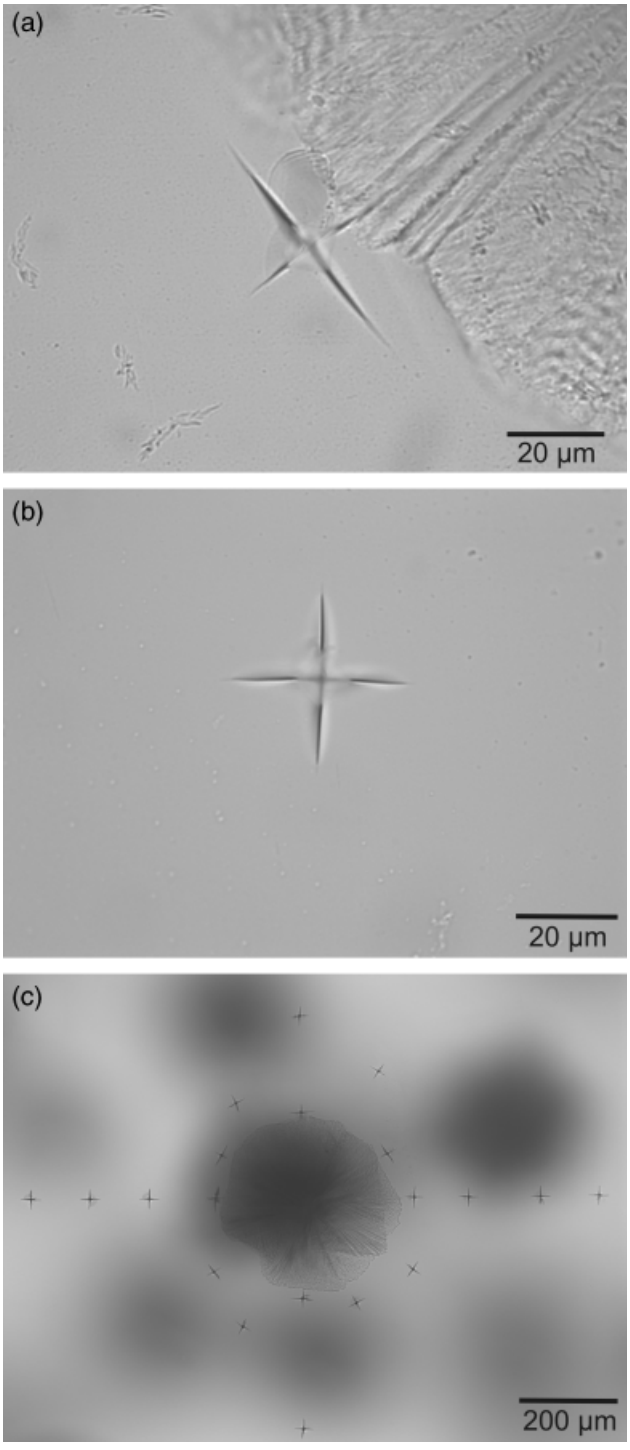


**Fig. 2.** Optical micrographs of 0.5 N Vickers indentations performed in air used for the determination of residual stresses (a) around a crystalline precipitate, (b) far from the precipitate, and (c) a general overview of the array of indentations performed in water.

A mathematical function similar to Eq. (4), $\sigma = \sigma_o(r/a)^{-3} + \sigma_B$, was fit to the stress data obtained in air. During the fitting process, a 95% confidence band was calculated around the fitted curve. Any data point outside this band was excluded and the fitting and the 95% confidence band were recalculated, and this process was repeated until no data were outside the confidence band.

The calculated coefficients $\sigma_o$ and $\sigma_B$ were $31 \pm 2$ MPa and $-3.6 \pm 0.8$ MPa for data in Fig. 3(a) and $-25 \pm 3$ MPa and $2 \pm 1$ MPa for data in Fig. 3(b), respectively. The magnitude of stress at the interface is related to the pressure $P$ predicted by Selsing's model according to Eq. (4) for the radial and tangential components. Therefore, the stress in the precipitate is predicted to be in the range of 31–50 MPa.

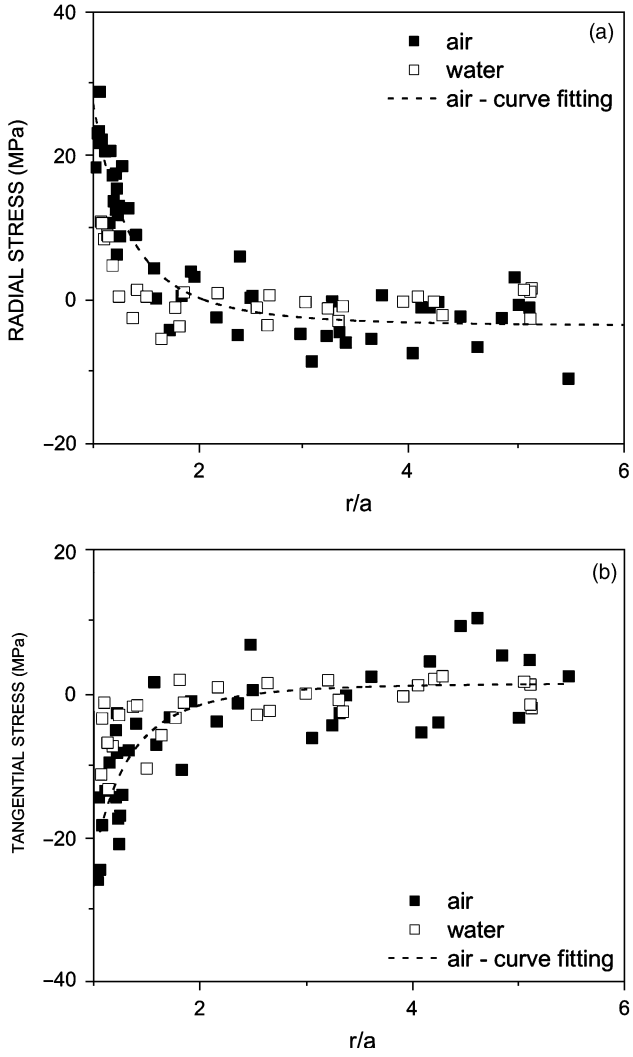


**Fig. 3.** (a) Radial and (b) tangential stresses as a function of the normalized distance $r/a$ as calculated using Eqs. (3*a*) and (3*b*) using the indentation technique for indentations in air and water, and curve fitting to air data.

The series of 1 N indentations performed inside precipitates of a partially crystallized sample produced an average crack length of $25 \pm 3$ μm, and on a fully crystallized sample produced radial cracks of $22 \pm 5$ μm. By using Eq. (3*a*) and assuming that the fully crystallized sample is a stress-free sample, a residual stress of only $10 \pm 20$ MPa is obtained by this method.

The determination of the crack profile as a function of depth was achieved by polishing the indentations with $CeO_2$. The amount of surface removal was determined by measuring the indentation diagonals of a large Vickers indentation during polishing and was estimated to be $0.32 \pm 0.02$ μm/min. Typical cracks of 0.5 N indentations are shown in Figs. 4(a) and (b) after 2 and 10 min of polishing. After 10–14 min, the majority of cracks around the indentations were not visible anymore. The main finding is that the generated crack is not semi-circular (as assumed in Eq. (3)), but has an elliptical shape with a length-to-depth ratio of 9.5 as shown in Fig. 4(c). The very significant implication of this geometry on the determination of residual stresses will be discussed in "Calculation of the Crack Geometry Factor."

### *(2) X-ray Diffraction Experiments*

The indentation technique allowed us to calculate the stress distribution in the glass matrix. To confirm the results, X-ray experiments were performed to estimate the stresses in the crystalline precipitates.

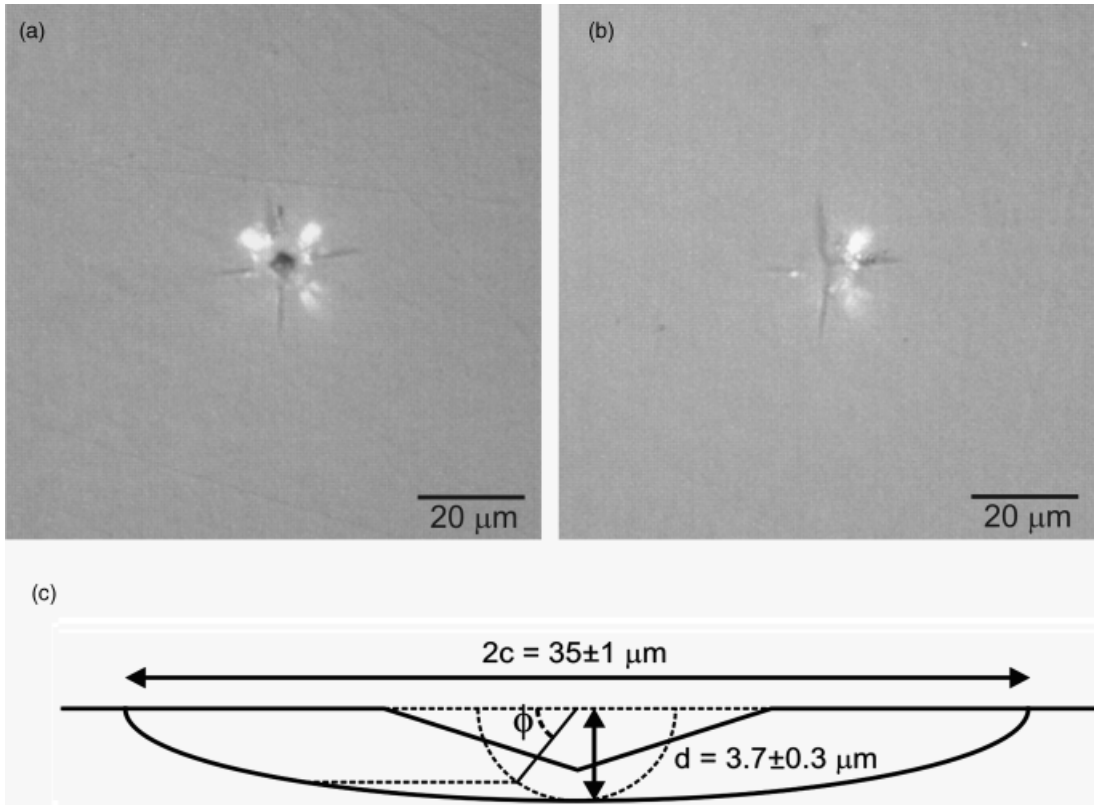


**Fig. 4.** Optical photographs of 0.5 N indentation on glass polished with $Ce_2O$ solution for (a) 2 min, (b) 10 min, and (c) crack dimensions. At 12 min of polishing, no cracks were visible for this indentation.

Figure 5 shows the experimental and the fitted X-ray profiles and the difference curve for partially crystallized samples in bulk (Fig. 5(a)) and powder form (Fig. 5(b)). The Si peak positions are well fitted, but this is not the case for the $Na_4Ca_4Si_6O_{18}$ peaks. In each figure shown in detail are the (404) and (40$\bar{4}$) reflections, which superimpose at the same 2θ angle. The peak positions of the fitted curve and the experimental data are displaced by $\sim 0.08^\circ$.

Figure 6 shows the experimental and fitted X-ray profiles for bulk (Fig. 6(a)) and powder (Fig. 6(b)) fully crystallized samples. The experimental data are reasonably fit by the simulated curves and the difference in the peak positions for the (404) and (40$\bar{4}$) reflections are not observed as they were for the partially crystallized samples.

To analyze the possible existence of texture, we compared the ratio of intensities of particular reflections among the different samples. The intensity ratio of the (220) and (404) peaks was chosen because of their high intensities. The ratio for each sample was compared with the theoretical value of 1.7 calculated from data of the ICSD database.[20] The values for the powder and bulk partially crystallized glass–ceramics are 1.7 and 4.2, respectively. For the powder and bulk fully crystallized samples, the values are 2.6 and 1.4, respectively. Therefore, a preferred orientation is observed with different degrees for all samples, with the exception of the partially crystallized powder sample.

The difference of $0.08^\circ$ observed for the partially crystallized samples might have its origin in a small distortion of the unit cell caused by the Na and Ca off-stoichiometry. Previously, it has been observed that off-stoichiometry of Na and Ca increases the cell parameter.[17,18] We observe here a possible distortion of the unit cell leading to a change in crystal symmetry. If the unit cell is hexagonal, the (404) and (40$\bar{4}$) peaks are superimposed. However, if the unit cell is slightly distorted, this distortion may promote the separation of (404) and (40$\bar{4}$) peaks. Possible transformations are from a hexagonal to a rhombohedral, monoclinic, or triclinic structure.[21]

The average strain of the $Na_4Ca_4Si_6O_{18}$ hexagonal unit cell can be defined as:

$$\bar{\varepsilon} = \frac{2}{3}\frac{\Delta a'}{a'} + \frac{1}{3}\frac{\Delta c'}{c'} \tag{7}$$

where $\Delta a'$ and $\Delta c'$ are the difference between the $a'$ and $c'$ parameters of stressed and stress-free specimens. The average stress in the crystalline phase for the fully crystallized sample can then be estimated by Hooke's law as

$$\sigma = E\bar{\varepsilon} \tag{8}$$

Table I shows the refined cell parameters and the calculated $\bar{\varepsilon}$ and σ for the fully crystallized sample assuming an average $E$ of 81 GPa.[5] The estimated residual stress is $30 \pm 9$ MPa.

An alternative method used to estimate the residual stress because of the differences of the experimental and calculated (404) and (40$\bar{4}$) profile peaks was simply to fit these peaks with a single Voigt function taking into account the Cu$K\alpha_1$–Cu$K\alpha_2$ components and to correct their positions with the aid of the Si peaks positions. The residual strain $\varepsilon_{hkl}$ is then calculated from Bragg's law differentiation as

$$\varepsilon_{hkl} = \frac{\Delta d_{hkl}}{d_{hkl}} = -\frac{\Delta(2\theta)}{2.\tan\theta} \tag{9}$$

where $\Delta d_{hkl}$ is the difference between the interplanar distance of the $hkl$ reflecting plane of the bulk sample and the powder, stress-free specimen.

To estimate the residual stress for the partially crystallized sample, a plane-stress state is assumed. Therefore, the calculated

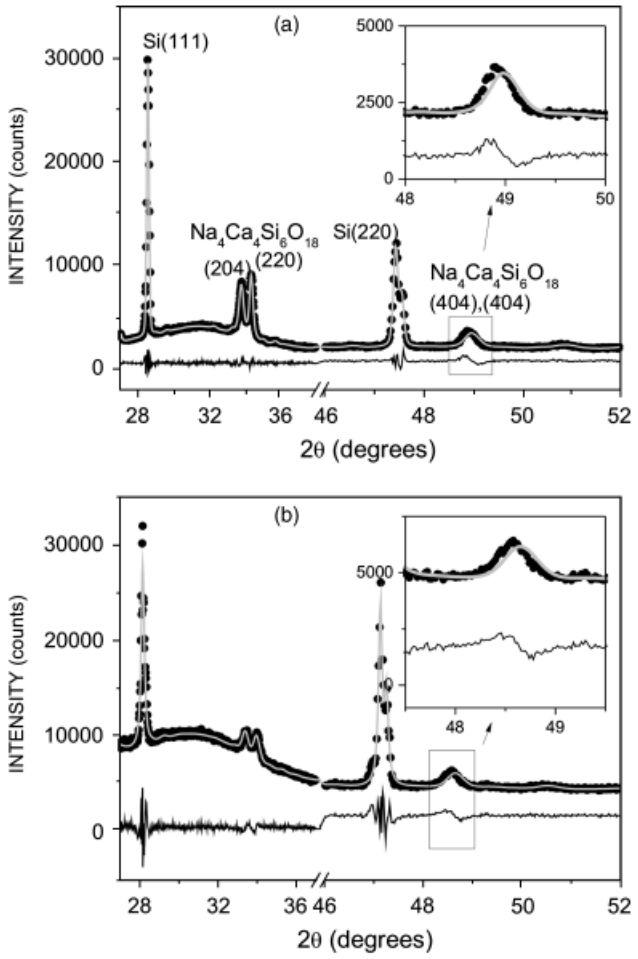


**Fig. 5.** Rietveld plots for (a) bulk and (b) powder partially crystallized samples. The intensity observed is represented by full circles, the calculated intensity and the difference curves are in light gray and black, respectively.

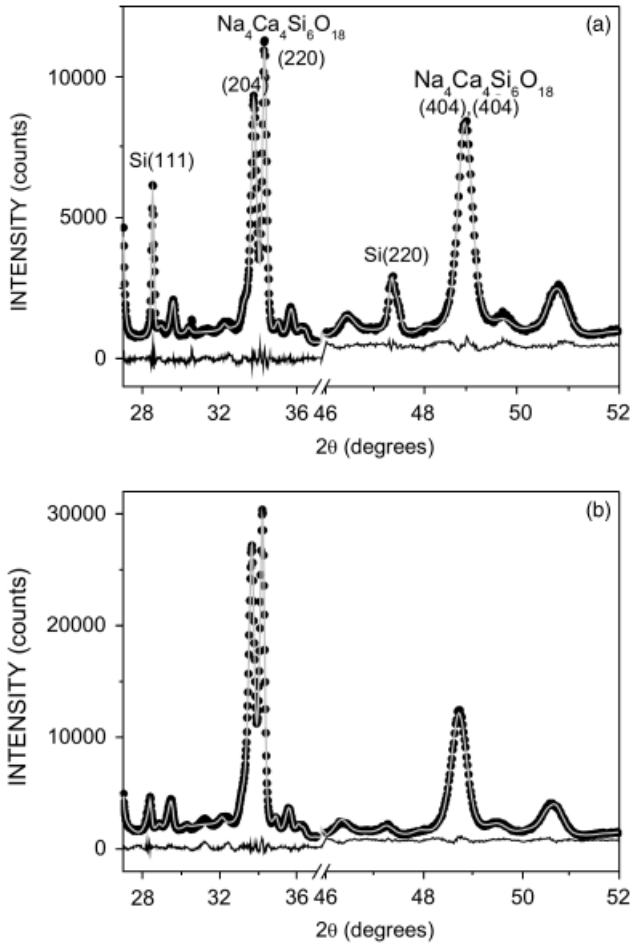


**Fig. 6.** Rietveld plots for (a) bulk and (b) powdered fully crystallized samples. The intensity observed is represented by full circles, the calculated intensity and the difference curves are in light gray and black, respectively.

stress is

$$\sigma_{hkl} = -\frac{E}{2\nu}\varepsilon_{hkl} \tag{10}$$

The justification of the assumption of plane-stress condition will be discussed in "Residual Stress Calculations in the Glass Matrix."

The residual stresses calculated by the fitting of the Voigt function of the (404) and (40$\bar{4}$) reflections are also shown in Table I. The residual stress for the fully crystallized sample was calculated according to Eq. (8) and was $50 \pm 20$ MPa, and agrees with the stress obtained by the Rietveld refinement (Table I). For the partially crystallized sample, the obtained residual stress was $130 \pm 80$ MPa. However, the residual stress at the interface estimated by the indentation technique was only in the 31–50 MPa range.

## V. Discussion

The residual stress at the crystal–glass interface measured by the indentation technique was between 31 and 50 MPa. But a much higher residual stress of $130 \pm 80$ MPa was estimated by X-ray diffraction. This last value agrees, within experimental error, with the average stress of 160 MPa estimated by Selsing's model and with earlier measurements of $154 \pm 50$ MPa using X-ray diffraction.[5]

It has been observed by X-ray diffraction experiments in a partially crystallized $Li_2O$–$2SiO_2$ glass–ceramic that the residual stresses are anisotropic.[22,23] Depending on the crystallographic direction, the residual stresses can either be positive or negative due to crystal anisotropy. It was also observed that the Selsing model can predict the variation of the residual stresses reasonably well with crystallographic direction if the thermal expansion coefficient for this particular crystallographic plane is used. In this study, the residual stress was estimated by X-ray diffraction by the shift in the (404) peak position by comparing bulk (stressed) and powder (stress-free) samples. This particular high-intensity reflection measures both the $a'$ and $c'$ lattice parameters variations (Eq. (7)) due to residual stress. Hence, the residual stress estimated in this way is a good representation of the average value in the crystalline precipitate.

Another possible variable that affects the measured residual stress is the glass composition *gradient* around the precipitates in samples with relatively small crystalline volume fractions.[17,18] In this particular case, the crystals are richer in $Na^+$ and depleted of $Ca^{2+}$ when compared with the stoichiometric composition, while the surrounded glass is consequently richer in $Ca^{2+}$ and depleted of $Na^+$ when compared with the stoichiometric glass. In turn, depletion of $Na^+$ in the glass phase around the crystals changes its thermal expansion coefficient. The glass composition near the interface can be estimated as $0.7Na_2O$–$2.2CaO$–$3SiO_2$,[18] and using the expressions given in Navarro,[24] the glass thermal expansion coefficient is reduced from $13.7 \times 10^{-6}$ to $12.3 \times 10^{-6}$ $K^{-1}$ in relation to the $1Na_2O \cdot 2CaO \cdot 3SiO_2$ stoichiometric glass ($P_2O_5$ was neglected here). However, this reduction increases the calculated residual stresses according to Selsing's model from 160 to 190 MPa. It is also possible that this chemical gradient slightly affects the glass elastic modulus, but this effect is probably small.

**Table I. Residual Stresses Calculated from Lattice Parameters Obtained by Fitting the Experimental X-Ray Patterns with the GSAS Program for Powder and Bulk Forms of Fully Crystallized Samples and from Corrected 2θ Angles for the (404) and (40$\bar{4}$) Reflections for Powder and Bulk Forms of Partially and Fully Crystallized Samples**

| Sample | Type | $a'$ (Å) | $c'$ (Å) | $\bar{\varepsilon}$(%) | $\sigma = E\varepsilon$ |
|---|---|---|---|---|---|
| Fully crystallized | Bulk | $10.4727 \pm 0.0002$ | $13.1324 \pm 0.0006$ | $0.04 \pm 0.01$ | $30 \pm 9$ MPa |
| | Powder | $10.4685 \pm 0.0002$ | $13.1281 \pm 0.0004$ | | |

| | | 2θ (°) | $\varepsilon_{404}$ (%) | $\sigma_{404} = E\varepsilon$ | $\sigma_{404} = -E\varepsilon/2\nu$ |
|---|---|---|---|---|---|
| Partially crystallized | Bulk | $48.743 \pm 0.007$ | $-0.09 \pm 0.05$ | | $130 \pm 80$ MPa |
| | Powder | $48.70 \pm 0.02$ | | | |
| Fully crystallized | Bulk | $48.771 \pm 0.002$ | $0.06 \pm 0.03$ | $50 \pm 20$ MPa | |
| | Powder | $48.80 \pm 0.01$ | | | |

The open issue on which the indentation model is more reliable for fracture toughness determination has been a matter of controversy for some time. Early work favored Eq. (1) given by Anstis and colleagues.[25,26] More recently, Niihara's expression (Eq. (6)) has been favored when compared with the Chevron notch method in glasses.[2] But some authors have argued that indentation methods are not valid.[3]

Here, we use Eq. (1) because it is the expression originally proposed by Zeng and Rowcliffe in their method to determine residual stresses. As the aim of our paper was to test their method to measure residual stresses in a glass–ceramic, we used Eq. (3) (that is derived from Eq. (1)). Equation (1) gives a lower value of $K_c$ ($0.37 \pm 0.03$ MPa$\cdot$m$^{1/2}$), which would further increase the discrepancy between the predictions of the indentation method and the measurement by an X-ray diffraction technique. Low $K_c$ values predicted by Eq. (1) have already been reported.[27–29] Here, Eq. (6) was preferred to estimate $K_c$ because the resulting value is closer to the toughness measured using the DCB geometry for a bio-glass.[30]

Regarding the use of Eq. (1) in the Zeng and Rowcliffe model, two points should be mentioned: (a) it assumes the relation $P \times c^{3/2}$ and (b) the crack geometry is considered as a 2D infinite crack at the surface, with a corresponding crack geometry factor of $\pi^{1/2}$. The first point was found to be valid for the experimental conditions of our work: the relation $P \times c^{3/2}$ is indeed obeyed above 0.2 N in a similar bio glass–ceramic.[31] For the second point, we propose a more realistic crack geometry factor based on a semi-elliptical surface crack.

Kese and Rowcliffe[32] have used a cube-corner indenter to estimate the residual stress field around a large Vickers indentation in soda–lime glass. The crack geometry was different than those assumed for Vickers indentation in earlier studies[8,9] and a new crack geometry factor was calculated for this method using a cube-corner indenter. The calculated stresses in the cube-corner experiments were a factor of 2–4 higher than the stresses calculated previously[8–9] and this was partially attributed to the varying stress field acting at the crack faces along the radial direction, and a difference in the cracks generated by the different indenters.

To the best of our knowledge, the nanoindentation technique has been used by only one group to estimate the residual stress field in a partially crystallized glass–ceramic.[33] However, the results were affected by the varying stress field along the radial direction and the crack length chosen to probe the stress field. The estimated stresses were much lesser than the expected (calculated and measured by other technique) values.

In order to thoroughly test the applicability of the indentation method of ZR for glass–ceramics, and in an attempt to explain the discrepancy observed in Soares and Lepienski,[33] in this article we investigated: (i) the effect of the *shape* of the indentation crack; and (ii) the development of a model that takes into account the fact that in the indentation method the precipitate is sitting on the sample *surface* (not fully embedded in the glass interior), and the hemisphere *shape* of the precipitate; two issues which were not considered in Selsing's model.

### *(1) Calculation of the Crack Geometry Factor*

The measured crack geometry of 0.5 N indentations shown in Fig. 4 is not semi-circular, but has a *semi-elliptical* shape with a length-to-depth ratio of 9.5. In this case, if we assume this length-to-depth ratio to be the same for the indentation cracks around the precipitates, the stress intensity factor at the crack tip is

$$K_c = \chi_r \frac{P}{c_1^{3/2}} + \Phi^* \sigma_t c_1^{1/2} \tag{11}$$

where the new crack geometry factor $\Phi^*$ for an semi-elliptical crack with length $2c$ and depth $d$ is[34]

$$\Phi^* = \frac{\sqrt{\pi}}{E\left(\frac{d}{c}\right)} F\left(\frac{d}{c}, \phi\right) \tag{12}$$

and

$$\begin{aligned} F &= M_1 g f_\phi \\ M_1 &= \sqrt{\frac{d}{c}}\left(1.13 - 0.09\frac{d}{c}\right) \\ g &= 1 + \frac{(1 - \sin^2\phi)}{10} \\ f_\phi &= \left[\left(\frac{d}{c}\right)^2 \cos^2\phi + \sin^2\phi\right]^{1/4} \\ E\left(\frac{d}{c}\right) &\cong \left[1 + 1.464\left(\frac{d}{c}\right)^{1.65}\right]^{1/2} \text{ for } \frac{d}{c} \le 1 \end{aligned}$$

In the above expressions, the crack depth is assumed to be much smaller than the sample thickness. As we are considering the point where the crack front meets the surface, $\phi = 0$, $g = 1.1$, $f_\phi = \sqrt{d/c}$ and the new crack geometry factor is:

$$\Phi^* = \left(\frac{d}{c}\right)\left[1.243 - 0.099\left(\frac{d}{c}\right)\right]\sqrt{\frac{\pi}{1 + 1.464\left(\frac{d}{c}\right)^{1.65}}} \tag{13}$$

The tensile and compressive residual stresses are given by Eq. (3) are rewritten as

$$\sigma_r = K_c \frac{1 - (c_0/c_1)^{3/2}}{\Phi^* c_1^{1/2}} \text{ (for tensile stress)} \tag{14a}$$

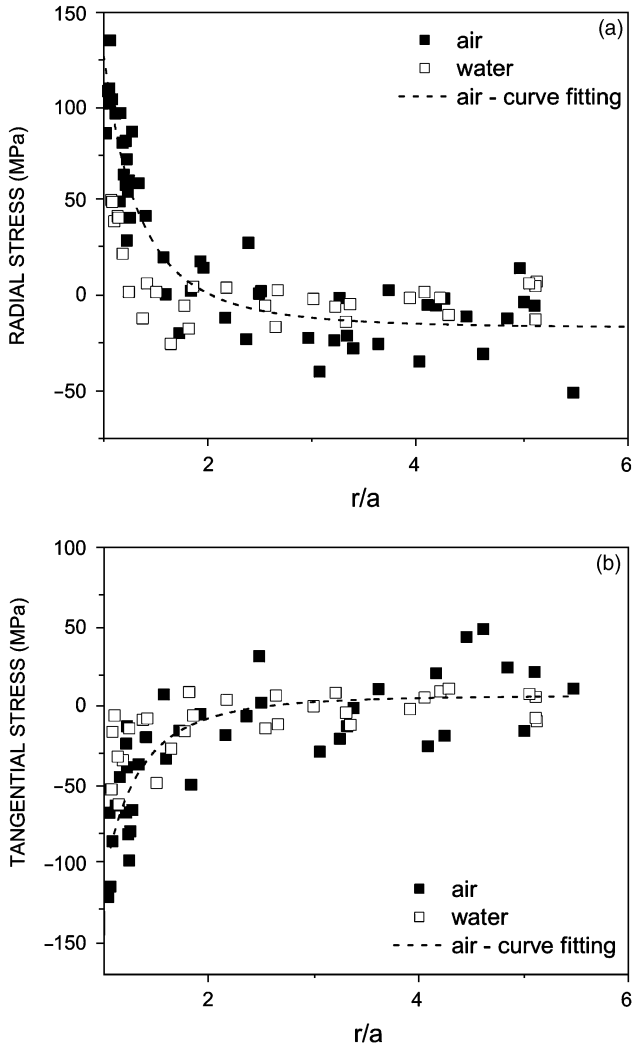


**Fig. 7.** (a) Radial and (b) tangential stresses as a function of the normalized distance $r/a$ calculated using Eqs. (14*a*) and (14*b*) using the indentation technique for indentations in air and water, and curve fitting to air data.

$$\sigma_r = -K_c \frac{1-(c_0/c_2)^{3/2}}{\Phi^* c_2^{1/2}} \text{ (for compressive stress)} \qquad (14b)$$

For our crack geometry, $d/c$ is 0.21 and the crack geometry factor $\Phi^*$ is $0.43 \pm 0.04$. The data shown in Figs. 3(a) and (b) are re-plotted with the corrected $\Phi^*$ and residual stresses given by Eq. (14) in Figs. 7(a) and (b). A function $\sigma = \sigma_o(r/a)^{-3} + \sigma_B$ is also fitted to the stress data obtained in air.

The constant $\sigma_0$ is $127 \pm 25$ MPa for the radial stress and $-102 \pm 17$ MPa for the tangential stress and is equal to the magnitude of the stress at the interface. Therefore, it can be used to estimate the pressure $P$ inside the precipitate according to Eq. (3). The radial stress predicts a hydrostatic stress inside the precipitate equals to $\sigma_0$, $127 \pm 25$ MPa, and is in agreement with the stresses predicted by Selsing's model and the value measured by X-ray diffraction.

The tangential stress data predict a stress $P$ inside the precipitate equal to $-2\sigma_0 = 204 \pm 34$ MPa. This value is higher than the predicted stresses by Selsing's model and X-ray diffraction experiments. One possible reason is that these cracks are short, and it is well established that radial cracks should be longer than $2.5b$, where $b$ is the half-impression diagonal, for the method (of estimating fracture toughness by indentation) to be valid.[13,25] Another possible reason is that these cracks in a radial direction are subjected by a stress gradient along their length. Portions of the crack closer to the precipitate experience higher compressive stresses than those farther apart. Meanwhile, the tangential cracks experience a constant stress along their length, allowing a more reliable stress measurement.

### *(2) Residual Stress Calculations in the Glass Matrix*

Selsing's model assumes that the spherical precipitate is completely surrounded by the matrix. The uniform residual stresses $P$ predicted by the model inside the precipitate shows a $1/r^3$ dependence outside. However, the model has some limitations when applied to our experiment. First, the precipitates are not spherical, they are hemispherical, and are located at the sample surface. The free surface relaxes some stress components and consequently the actual stress tensor might be different from those calculated by the Selsing's model. Therefore, a more suitable theoretical framework should be used so that the hemispherical precipitates and their location are taken into account.

Mindlin and Cheng[35] developed equations for the displacements of a center of dilatation in a semi-infinite matrix and applied them for a spherical inclusion near the surface. Their results were further developed by Hu,[36] based on Mindlin and Cheng's displacement equations, who calculated analytically the strain and stress tensors for a parallel-epipedic thermal inclusion in a three-dimensional half-space.

According to Hu,[36] the stresses produced at point $(x, y, z)$ by a parallelepipedic strain nucleus at $(x', y', z')$ are, in the coordinate system defined in Fig. 8:

$$\begin{aligned}
\sigma_{xx} =& 2GP\{r_1^{-3} + (3-8\nu)r_2^{-3} - 3\bar{x}^2 r_1^{-5} - 3[(3-4\nu)\bar{x}^2 \\
&+ 2z\hat{z} - 4\nu\hat{z}^2]r_2^{-5} + 30z\hat{z}\bar{z}^2\bar{x}^2 r_2^{-7}\} \\
\sigma_{yy} =& 2GP\{r_1^{-3} + (3-8\nu)r_2^{-3} - 3\bar{y}^2 r_1^{-5} - 3[(3-4\nu)\bar{y}^2 \\
&+ 2z\hat{z} - 4\nu\hat{z}^2]r_2^{-5} + 30z\hat{z}\bar{z}^2\bar{y}^2 r_2^{-7}\} \\
\sigma_{zz} =& 2GP\{r_1^{-3} - r_2^{-3} - 3\bar{z}^2 r_1^{-5} + 3\hat{z}(\hat{z}-6z)r_2^{-5} + 30z\hat{z}^3 r_2^{-7}\} \\
\sigma_{xy} =& -6GP\bar{x}\bar{y}[r_1^{-5} + (3-4\nu)r_2^{-5} - 10z\hat{z}r_2^{-7}] \\
\sigma_{xz} =& -6GP\bar{x}[\bar{z}r_1^{-5} + (2z+\hat{z})r_2^{-5} - 10z\hat{z}^2 r_2^{-7}] \\
\sigma_{yz} =& -6GP\bar{y}[\bar{z}r_1^{-5} + (2z+\hat{z})r_2^{-5} - 10z\hat{z}^2 r_2^{-7}]
\end{aligned} \qquad (15)$$

where

$$\begin{aligned}
\bar{x} =& x - x' \\
\bar{y} =& y - y' \\
\bar{z} =& z - z' \\
\hat{z} =& z + z' \\
r_1^2 =& \bar{x}^2 + \bar{y}^2 + \bar{z}^2 \\
r_2^2 =& \bar{x}^2 + \bar{y}^2 + \hat{z}^2 \\
P =& \Delta\alpha\Delta T \frac{(1+\nu)}{4\pi(1-\nu)} dx'dy'dz'
\end{aligned} \qquad (16)$$

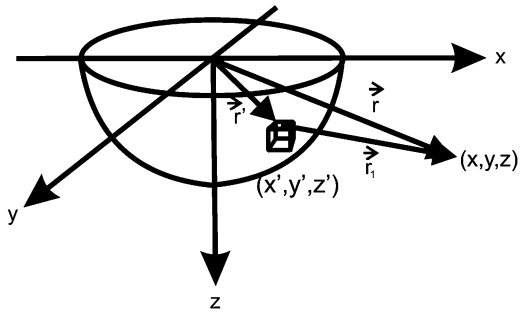


**Fig. 8.** Schematic representation of a hemispherical inclusion at the surface and the coordinate system.

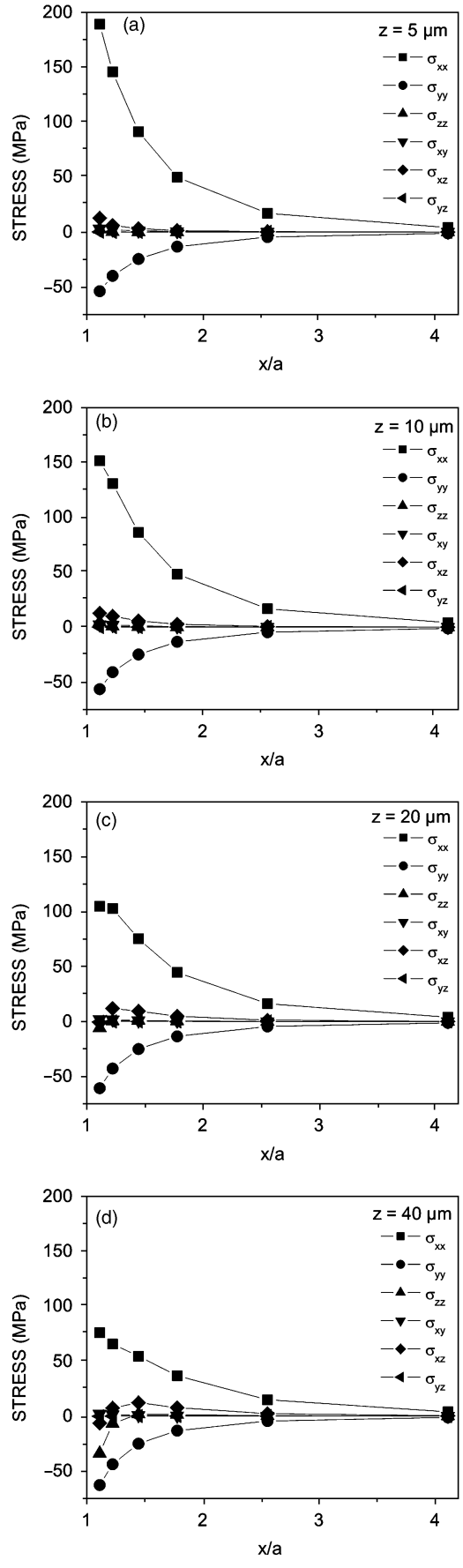


**Fig. 9.** Magnitude of stresses with distance from the precipitate at different depths of (a) 5 μm, (b) 10 μm, (c) 20 μm, and (d) 40 μm.

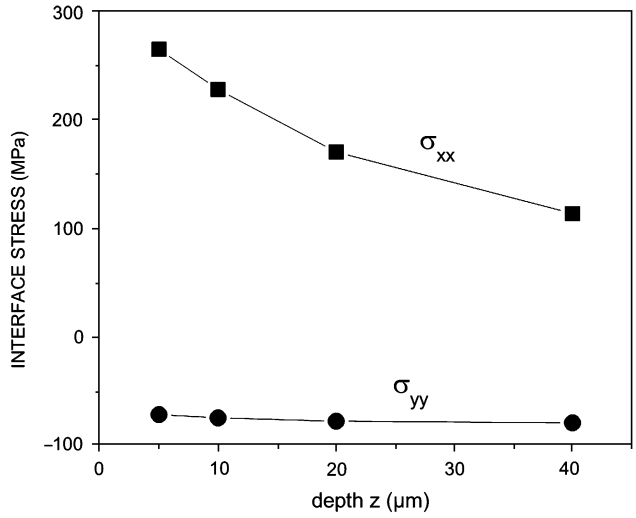


**Fig. 10.** Variation of $\sigma_{xx}$ and $\sigma_{yy}$ with a depth close to the interface at $x = 180$ μm.

where $\Delta\alpha$ is the thermal expansion difference between the glass and the matrix, $\Delta T$ is the temperature difference, and $\nu$ and $G$ are the Poisson ratio and shear modulus, respectively.

This model was applied by dividing the hemispherical inclusion in small elements $dx'dy'dz'$. The total stresses at a particular point were obtained by numerical integration over the total volume inclusion. In Hu's model, it is assumed the elastic constants of the precipitate and the matrix are the same. For the stress estimation, the elastic constants of the glass and crystal were assumed as $\nu = 0.27$, $\alpha_m = 13.7 \times 10^{-6}$ $K^{-1}$, $\alpha_p = 20.5 \times 10^{-6}$ $K^{-1}$, $\Delta T = 310$ K, and $G = 31.9$ GPa.

The conditions assumed for the numerical calculations were as close as possible to the experiments. The hemispherical precipitate radius was 180 μm and each element of the grid was a cube of 10 μm × 10 μm × 10 μm. The stresses were estimated up to a depth of 40 μm, i.e. the depth probed by the indentation technique.

The results are shown in Fig. 9. The stress state can be defined as a plane-stress condition. The component normal to the surface $\sigma_{zz}$ is null near the surface as are the other shear stresses. The radial component $\sigma_{xx}$ is tensile and decreases with depth. The tangential component $\sigma_{yy}$ is compressive and increases slightly with depth. All the shear stresses are approximately zero at all depths.

The curves in Fig. 9 can be extrapolated towards the interface ($x = a$) assuming a power law function. In this case, the radial and tangential components $\sigma_{xx}$ and $\sigma_{yy}$ close to the crystal/glass interface are shown in Fig. 10. The radial component is 270 MPa nearby the surface and decreases with the increasing depth. The tangential component does not vary with depth, being approximately −75 MPa. For comparison, the predicted average residual stress by Selsing's model is 160 MPa. Near the surface, the radial component is higher than that predicted by Selsing's model. Therefore, in this "surface" model, the radial stress component in a crystal on a glass surface is approximately 70% *larger* than the radial stress produced by a spherical precipitate deep inside the glass matrix. The tangential stress $\sigma_{yy}$ is not affected.

## VI. Conclusions

Residual stresses in the glass matrix around crystalline precipitates in a bio glass-ceramic were determined by the Vickers indentation technique of Zeng and Rowcliffe. If the crack morphology is assumed as surface line cracks (as in the original model), the estimated stress is much lower than the stresses measured by X-ray diffraction (in the crystals) and predicted by

Selsing's model. A correction for the crack geometry factor assuming a *semi-elliptical* crack shape restores the agreement between the experimental residual stresses and the values measured by XRD and theoretically predicted. Thus, if a proper account of the real crack geometry is taken, the indentation technique of ZR can be successfully used.

In addition, a numerical model for the calculation of residual stress that takes into account the hemispherical shape of a crystalline precipitate at a free surface was developed. Estimates show that the radial component of the residual stress is enhanced by 70% near the sample surface in comparison with the internal residual stress calculated by Selsing's model, whereas the tangential stresses are not affected.

## Acknowledgments

The authors appreciate CNPq/Brazil—process no. 151917/2006-0 and Fapesp/Brazil—contract no. 07/08179-9 for the financial support of this research. One of the authors (F. C. S.) acknowledges many fruitful discussions on X-ray data refinement with Prof. C. O. Paiva-Santos.

## References

[1]O. Peitl, E. D. Zanotto, and L. L. Hench, "Highly Bioactive $P_2O_5$–$Na_2O$–CaO–$SiO_2$ Glass–Ceramics," *J. Non-Cryst. Solids*, **292**, 115–26 (2001).

[2]O. Peitl, G. La Torre, and L. L. Hench, "Effect of Crystallization on Apatite Layer Formation of Bioactive Glass 45S5," *J. Bio. Mater. Res.*, **30**, 509–14 (1996).

[3]T. Kokubo, "A/W Glass–Ceramic: Processing and Properties" pp. 75–88 in *An Introduction to Bioceramics, Ch. 5*, Edited by L. L. Hench, and J. Wilson. World Scientific, Singapore, 1993.

[4]L. L. Hench and J. K. West, "Biological Applications of Bioactive Glasses," *Life Chem. Rep.*, **13**, 187–241 (1996).

[5]V. R. Mastelaro and E. D. Zanotto, "Residual Stresses in a Soda–Lime–Silica Glass–Ceramic," *J. Non-Cryst. Solids*, **194**, 297–304 (1996).

[6]L. Grabner, "Spectroscopic Technique for the Measurement of Residual Stress in Sintered $Al_2O_3$," *J. Appl. Phys.*, **49**, 580–3 (1978).

[7]J. W. Zwanziger, U. Werner-Zwanziger, E. D. Zanotto, E. Rotari, L. N. Glebova, L. B. Glebov, and J. F. Schneider, "Residual Internal Stress in Partially Crystallized Photo Thermo Refractive Glass: Evaluation by Nuclear Magnetic Resonance Spectroscopy and First Principles Calculations," *J. Appl. Phys.*, **99**, 083511, 6pp (2006).

[8]K. Zeng and D. J. Rowcliffe, "Experimental Measurement of Residual Stress Field Around a Sharp Indentation in Glass," *J. Am. Ceram. Soc.*, **77**, 524–30 (1994).

[9]K. Zeng and D. J. Rowcliffe, "Vickers Indentations in Glass—II. Comparison of Finite Element Analysis and Experiments," *Acta Metall. Mater.*, **43**, 1945–54 (1995).

[10]K. Zeng and D. J. Rowcliffe, "Vickers Indentations in Glass—I. Residual Stress Fields and Iso-Stress Contour Maps," *Acta Metall. Mater.*, **43**, 1935–43 (1995).

[11]J. Selsing, "Internal Stresses in Ceramics," *J. Am. Ceram. Soc.*, **44**, 419 (1961).

[12]R. W. Davidge and T. J. Green, "The Strength of Two-Phase Ceramic/Glass Materials," *J. Mater. Sci.*, **3**, 629–34 (1968).

[13]K. Niihara, R. Morena, and D. P. H. Hasselman, "Evaluaton of $K_{IC}$ of Brittle Solids by the Indentaton Method with Low Crack-to-Indent Ratios," *J. Mater. Sci. Lett.*, **1**, 13–6 (1982).

[14]W. C. Oliver and G. M. Pharr, "An Improved Technique for Determining Hardness and Elastic Modulus Using Load and Displacement Sensing Indentation Experiments," *J. Mater. Res.*, **7**, 1564–83 (1992).

[15]A. C. Larson and R. B. Von Dreele, "General Structure Analysis System (GSAS)," Los Alamos National Laboratory Report LAUR 86-748 (2004).

[16]B. H. Toby, "EXPGUI, a Graphical User Interface for GSAS," *J. Appl. Cryst.*, **34**, 210–3 (2001).

[17]V. M. Fokin, O. V. Potapov, E. D. Zanotto, F. M. Spiandorello, V. L. Ugolkov, and B. Z. Pevzner, "Mutant Crystals in $Na_2O \cdot 2CaO \cdot 3SiO_2$ Glasses," *J. Non-Cryst. Solids*, **331**, 240–53 (2003).

[18]V. M. Fokin, O. V. Potapov, V. L. Ugolkov, E. D. Zanotto, and F. M. Spiandorello, "The Kinetics of Crystallization of Solid Solutions in a Glass of the Stoichiometric Composition $Na_2O \cdot 2CaO \cdot 3SiO_2$," *Russian J. Phys. Chem.*, **77**, 1639–41 (2003).

[19]D. C. Clupper, J. E. Gough, P. M. Embanga, I. Notingher, L. L. Hench, and M. M. Hall, "Bioactive evaluation of 45S5 bioactive glass fibres and preliminary study of human osteoblast attachment," *J. Mater. Sci.-Mater. Med.*, **15**, 803–8 (2004).

[20] Card 61241, ICSD—Inorganic Crystal Structure Database, FIZ Karlsruhe, Germany, 2008.

[21]B. D. Cullity, *Elements of X-Ray Diffraction*, 2nd edition, p. 501. Addison-Wesley Publishing Company, Reading, MA, 1978.

[22]V. R. Mastelaro and E. D. Zanotto, "Anisotropic Residual Stresses in Partially Crystallized $Li_2O$–$2SiO_2$ Glass–Ceramics," *J. Non-Cryst. Solids*, **247**, 79–86 (1999).

[23]H. Pinto, L. Ito, M. Crovace, E. B. Ferreira, F. Fauth, T. Wroblewski, E. D. Zanotto, and A. R. Pyzalla, "Surface and Bulk Residual Stresses in $Li_2O \cdot 2SiO_2$ Glass–Ceramics," *J. Non-Cryst. Solids*, **353**, 2307–17 (2007).

[24]J. M. F. Navarro, *El Vidrio*, 2nd edition, p. 388. Consejo Superior de Investigaciones Científicas, Fundación Centro Nacional del Vidrio, Madrid, Spain, 1991.

[25]G. R. Anstis, P. Chantikul, B. R. Lawn, and D. B. Marshall, "A Critical Evaluation of Indentation Techniques for Measuring Fracture Toughness: I, Direct Crack Measurements," *J. Am. Ceram. Soc.*, **64**, 533–8 (1981).

[26]D. K. Shetty, A. R. Rosenfield, and W. H. Duckworth, "Indenter Flaw Geometry and Fracture Toughness Estimates for a Glass–Ceramic," *J. Am. Ceram. Soc.*, **68**, C-282–4 (1985).

[27]P. Vullo and M. J. Davis, "Comparative Study of Micro-Indentation and Chevron Notch Fracture Toughness Measurements of Silicate and Phosphate Glasses," *J. Non-Cryst. Solids*, **349**, 180–4 (2004).

[28]G. D. Quinn and R. C. Bradt, "On the Vickers Indentation Fracture Toughness Test," *J. Am. Ceram. Soc.*, **90**, 673–80 (2007).

[29]J. J. Kruzic, D. K. Kim, K. J. Koester, and R. O. Ritchie, "Indentation Techniques for Evaluating the Fracture Toughness of Biomaterials and Hard Tissues," *J. Mech. Behav. Biomed. Mater.*, **2**, 384–95 (2009).

[30]D. R. Bloyer, J. M. McNaney, R. M. Cannon, E. Saiz, A. P. Tomsia, and R. O. Ritchie, "Stress–Corrosion Crack Growth of Si–Na–K–Mg–Ca–P–O Bioactive Glasses in Simulated Human Physiological Environment," *Biomaterials*, **28**, 4901–1 (2007).

[31]J. A. Nychka, D. Li, and B. Alexander, "In Vitro Bioactivity of 45s5 Bioactive Glass as a Function of Indentation Load," *J. Mech. Behav. Biomed. Mater.*, **1**, 243–51 (2008).

[32]K. Kese and D. J. Rowcliffe, "Nanoindentation Method for Measuring Residual Stress in Brittle Materials," *J. Am. Ceram. Soc.*, **86**, 811–6 (2003).

[33]P. C. Soares Jr. and C. M. Lepienski, "Residual Stress Determination on Lithium Disilicate Glass–Ceramic by Nanoindentation," *J. Non-Cryst. Solids*, **348**, 139–43 (2004).

[34]Y. Murakami, *Stress Intensity Factors Handbook*, Vol. 2, 1st edition, p. 714. Pergamon, Oxford, 1987.

[35]R. D. Mindlin and D. H. Cheng, "Thermoelastic Stress in the Semi-Infinite Solid," *J. Appl. Phys.*, **21**, 931–3 (1950).

[36]S. M. Hu, "Stress from a Parallelepipedic Thermal Inclusion in a Semispace," *J. Appl. Phys.*, **66**, 2741–3 (1989). □